EVLA Memo 235
Testing Ionospheric Faraday Rotation Measure Models

Rick Perley, Eric Greisen, Lilia Tremou, and Bryan Butler
National Radio Astronomy Observatory, Socorro, NM
and
Tony Willis
Dominion Radio Astrophysical Observatory, Penticton BC

October 21, 2024

Abstract

We test the accuracy of ionospheric Faraday rotation measure estimates derived from global models of the vertical total electron content using the AIPS task TECOR, and from two versions using a regional model derived from ground station data using the ALBUS program. We use six VLA P-band lunar observations to make these tests. We find that all models remove the day/night change in Ionospheric Faraday Rotation Measure (IFRM) with an accuracy better than 0.1 rad/m^2. However, all global models introduce an offset in the IFRM of 0.5 to 1.0 rad/m^2. This offset varies from day to day, and is nearly constant within a given observation. Both of the regionally-derived ALBUS IFRM estimates are closer to the actual IFRM than any of the global models. Based on these observations, the ALBUS model provides IFRM estimates correct to ~ 0.2 rad/m^2.

1 Background

Earth's magnetized ionosphere introduces a rotation of the plane of polarization for incoming radiation due to the Faraday effect. The rotation amount is given by $\Delta\chi = \text{IFRM} \times \lambda^2$ radians, where IFRM, the ionospheric Faraday rotation measure, is in rad/m^2, and the wavelength λ is in meters. Typical IFRMs during quiet sun conditions are from 0.5 (night) to 2 (day) rad/m^2, and can reach 6 rad/m^2 or more when the sun is active. These rotations, which can occur on timescales of hours to minutes, are a significant barrier to enabling accurate meter-wavelength polarimetry. To enable this, removal of the IFRM with an accuracy of at least 0.2 rad/m^2 is necessary.

The AIPS [G2003] program TECOR, authored by Chris Flatters in the late 1990s, generates estimates of the IFRM which can be applied to data to correct the polarization angle. It does this by utilizing global model estimates of the vertical total electron content (VTEC) available from the CDDIS (Crustal Dynamics Data Interchange System) website, combined with the IGRFv13 model of the Earth's magnetic field [A2021], assuming that the electrons are all in a thin shell at a height of 450 km. This height is assumed because it is roughly the appropriate height for a thin shell approximation over a wide variety of conditions and in mid-latitudes [Z2019]. In EVLA Memo#230 [PG2024], Perley and Greisen utilized VLA P-band polarimetric observations of the Moon to show that when the jplg global model VTEC values are utilized, the resulting IFRM estimates are consistently too high by a value of typically 0.5 to 1.0 rad/m^2.

This overestimate is due to an offset in rotation measure, as the model estimates are very effective in removing the diurnal changes in the observed EVPA (electric vector position angle) of polarized sources. Stated another way, the model estimates, when applied to the observations, uniformly overrotate the EVPA corrections of all sources by an amount given by $\sim 0.7\lambda^2$ radians – a value which varies little over the length of an observation or from source to source, but varies significantly between observations taken on different days. This apparent excess IFRM cannot be caused by the Faraday rotation in the cis-lunar space between the Moon and the height of the Global Navigational Satellite System (GNSS) satellites, nor can it be due to the lunar thermal emission responsible for the observed radio emission. Memo#230 concluded that this excess is due to either errors in the calibration/imaging software, or errors in the estimates of the ionospheric VTEC.

This memo extends the work presented in EVLA Memo#230 by comparing the IFRM estimates of thin shell models utilized seven different sources of global VTEC maps, and two regional models, to the actual IFRM values determined from six observations of the Moon.

2 Method

Judging the accuracy of the IFRM estimates requires observing polarized sources with known intrinsic EVPA at all wavelengths. At meter-wavelengths, the only source known to us with both a known EVPA and sufficient polarized brightness to be visible to the VLA is the Moon. The lunar radio emission originates from 10 – 20λ beneath the surface. The passage of this unpolarized thermal radiation through the lunar surface causes it to become radially polarized, reaching a degree of nearly 30% near the limb[1]. The proximity of the Moon enables, despite its low surface brightness, useful polarimetric imaging by the VLA at P-band when in its 'C' and 'D' configurations[2]. The lunar emission provides enough polarized flux density with ∼arcminute resolution to enable IFRM measurements on timescales of ∼ 30 minutes or longer.

In principle, an estimate of the IFRM requires knowing the precise electron density and magnetic field distributions along the path through the ionosphere from the VLA to the Moon at the time of observation. These, in turn, require knowing the full 4-dimensional (longitude, latitude, altitude, and time) distribution of electron density and magnetic field – a very difficult prospect. Because of this, traditionally (at least in radio astronomy), simpler approximations have been used involving available global VTEC maps (as a function of longitude, latitude, and time) a current model of the magnetic field, and a thin shell approximation for the ionospheric electrons. As noted above, the AIPS task TECOR uses this approach. Alternatives include ionFR (which reads the height of the thin shell from the VTEC files, which are in the IONEX format) [S2013], and RMextract (developed at ASTRON) [M2018]. The VTEC global model files are developed by various different Ionospheric Associated Analysis Centers (IAACs) of the International GNSS Service (IGS), using timing data from the GNSS constellations and a network of globally distributed ground stations. A useful introduction to how GNSS timing data are employed to estimate IFRM values is given by [E2001].

An alternative regional model is provided by the program 'ALBUS' (Advanced Long Baseline User Software), developed by James Anderson [W2014]. Originally intended to enable phase corrections for VLBI observations, the program has been modified to enable IFRM estimates. ALBUS derives a local estimate of the IFRM using the GNSS timing data from ground stations within a few hundred kilometers of a specified location, and a realistic distribution of electron density with height. For the VLA, there are approximately a dozen ground stations within a radius of 300 km which can be utilized for model fitting.

Due to its large angular size and low brightness, the Moon is a very challenging object to image at P-band with the VLA in its compact D and C configurations. It is completely resolved out in the high resolution A and B configurations. Its large angular size makes it quite unsuitable as a polarization calibrator for general work, so it is important to establish a network of secondary polarization calibrators which can be used in any array configuration. Desirable attributes for such calibrators will be: compact size, high polarized flux density, stable flux density (including polarized flux density), low intrinsic rotation measure, and a sky distribution making at least one source available for use at any time. For these proposed secondary sources, we need to determine the intrinsic EVPAs as a function of frequency. At the time of the observations reported in this memo, only three good candidates were known – DA240, 3C303, and 3C345. Results for those sources from these observations will be presented in a separate memo.

3 The Observations

The data utilized in this memo are from six VLA P-band observations of the Moon and three known compact polarized sources: DA240, 3C303, and 3C345. Details of these observations are shown in Table 1. In this table, the second column gives the array configuration used for the observation, and the third column gives a code which is used throughout this memo to identify which observation is being discussed. Column 6 give the angular offset between the Moon and the Sun, and column 7 gives the on-source integration time in minutes. The last three columns give the observation start, lunar transit, and stop times.

The first four P-band observations were taken with the full suite of 16 spectral windows, each of 16 MHz width, spanning 224 – 480 MHz. However, due to RFI, eight of these cannot be used. The eight remaining are in two blocks of four: The lower spans 288 – 352 MHz, the upper spans 388 – 448 MHz. The last two ('D2', and 'DC') observations utilized only the eight relatively RFI-free spectral windows. The observations were taken with 125 kHz frequency resolution and with 2 or 3 seconds time resolution.

[1] The physics of this process are explained at length in [PB2013]

[2] Venus and Mars are also good candidates for absolute polarimetry, but are too distant to provide sufficient flux density for P-band observations.

Table 1: **Observation Log for the VLA P-band Lunar Observations**

1	2	3	4		5		6	7	8	9	10
Date	Conf.	Code	Sun		Moon		Sep^n	IntTime	Start	Transit	End
			RA	Dec	RA	Dec	deg	min	MST		
10May2017	D	D1	03 09	17 40	14 45	-10 58	171	120	21:30	23:30	01:50
06Aug2017	C	C1	09 04	16 42	19 52	-18 27	162	280	19:40	23:00	03:15
30Dec2018	C	C2	18 36	-23 10	13 24	-03 15	75	450	01:55	07:10	12:20
13Dec2022	C	C3	17 21	-23 08	09 34	19 51	122	320	00:45	04:05	08:15
04Nov2023	D	D2	14 36	-15 16	08 24	24 39	100	210	03:05	05:30	08:10
20Jan2024	D→C	DC	20 10	-20 04	04 17	25 06	124	220	15:40	20:30	23:37

4 Calibration

Data were calibrated in AIPS using standard methods, utilizing the programs FRING, CLCAL, BPASS, CALIB, RLDLY, and PCAL. As the P-band receivers are linearly polarized, all calibration steps noted above utilized known unpolarized sources[3]. The final calibration step – removing the cross-hand phase – uses the program 'VHDIF', and requires a strongly polarized source. We utilized DA240 for all observations except C1, which used 3C345, as DA240 was below the horizon for that observation.

Following editing and calibration, all data were decimated in frequency to 1 MHz channelwidth, and in time to 10 or 12 seconds to facilitate imaging.

5 Ionospheric Corrections

Estimates of the IFRM were generated for all six observations using both TECOR and ALBUS. In addition, we have used ASTRON's RMextract program for comparison to the estimates of TECOR.

5.1 Thin Shell Models Utilizing Gobal VTEC Maps

Many organizations publish global maps of the VTEC using timing data from GNSS satellites received by a few hundred globally-distributed ground stations. These maps provide the VTEC column density on a 2.5 by 5.0 degree grid (latitude, longitude), at an effective height of 450 km, typically on time scales from 30 minutes to two hours. We have utilized seven of these maps provided by the organizations listed below in Table 2 along with details of each. In this table, column 1 lists the identification code, column 2 gives the responsible organization, and column

Table 2: **Global Model Characteristics**

1	2	3	4	5	6	7
Name	Organization	ElCutoff	#Sat	SatConst	#Sta	TimeStep
jplg	Jet Propulsion Laboratory	10	32	G	170	2
codg	Center for Orbit Determination in Europe	10	79	G,E	235	1
esag	European Space Operations Center	10	78	G,E	248	2
igsg	Geodynamics Research Lab, GRL/UWN	0	31	G	297	2
upcg	Polytechnic Univerisity of Catalonia	0	54	G,E	235	2
casg	Chinese Academy of Science	0	108	G,C,E,R	?	0.5
emrg	Space Weather Canada	10	52	G,R	270	1

3 shows the elevation cutoff employed for the model. Column 4 lists the typical number of satellites utilized in the modelling, and column 5 lists the GNSS constellations used in the modelling: 'G' = GPS, the US Global Positioning System with up to 30 satellites, 'E' = the European Unions's Galileo, with 27 active satellites, 'C' = China's BeiDou Navigation Satellite System (BDS), with up to 28 satellites, and 'R' = Russia's Global Navigation Satellite System

[3]Gain calibration using a polarized source will completely remove its linear polarization!

(GLONASS), with 24 satellites[4]. Column 6 gives the number of ground stations used for modelling. All numbers vary slightly from observation to observation. Note that the igsg model is a combination of the codg, jplg, and upcg maps, seemingly using only the GPS satellites. The number of ground stations in the casg maps is not listed in their IONEX databases, but appears to be similar to the other models. Column 7 gives the time cadence of the maps in hours. Maps on a more rapid timescale are also available – for example, there is a 'uqrg' map, providing maps on a 15-minute cadence which we have utilized for the results shown in Section 7.3.

Examples of the calculated IFRMs for the six VLA observations, for the Moon and the polarized calibrators, are shown in Fig 1. These maps have utilized the jplg global map with the IGRFv13 magnetic field model.

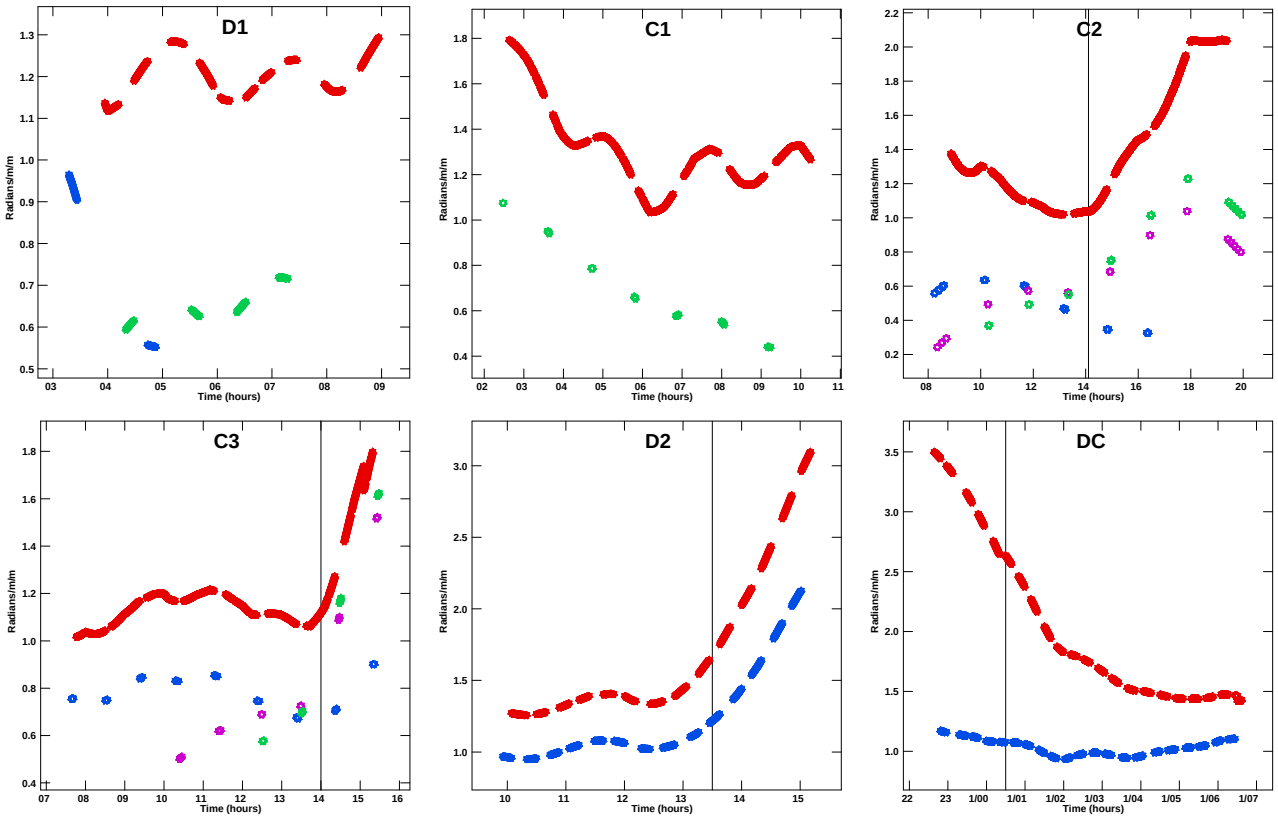

Figure 1: The TECOR estimates of the IFRM as a function of IAT time in hours for each of the six observations, using the jplg global VTEC model data. Sources are color-coded: the Moon in red, DA240 in blue, 3C303 in purple, and 3C345 in green. The thin vertical line in the C2, C3, and D2 panels indicate the time of sunrise, and sunset in the DC panel.

5.2 ALBUS

ALBUS is a collections of programs (in FORTRAN, C++, and Python) written by James Anderson (with contributions by others) which generates a model of the IFRM at a given location and for particular directions, as a function of time. It does this by utilizing GNSS timing data from ground stations within a specified distance of the given location along with a parametrically generated ionospheric vertical distribution of electrons. Originally developed to calculate dispersive delays for removal of ionospheric phase variations from VLBI data, it was modified to enable IFRM calculations. As it is a regional model, utilizing local data, we expect it to be better able to track local variations in the IFRM on scales smaller than the 2.5 x 5 degree sampling provided by the global models.

ALBUS works by collecting RINEX (Receiver Independent Exchange Format) data that are sent from ground station receivers to central repositories. ALBUS utilizes a database of some 3000 stations situated across the globe. Not all stations in the database send RINEX files to central repositories and some stations can disappear and new stations can appear over time.

[4]These values come from the Wikipedia article on Satellite Navigation.

Passage of GNSS signals through the ionosphere introduces a wavelength-dependent delay due to the ionized medium. In order to determine the exact delay due to the ionosphere, satellite and receiver-dependent timing offsets must be removed. After the timing data from the RINEX files are collected, ALBUS first goes through an extensive procedure to adjust and correct the timing data for these offsets (DCBs – differential clock bias). ALBUS obtains these biases from the codg IONEX files. Not all available ground stations are included in the codg IONEX data – we are uncertain whether ALBUS uses these uncorrected data in the modelling, or tries to determine the DCBs.

After collecting and correcting the RINEX data, ALBUS creates a general model of the ionosphere in the region over the telescope as a function of time from the beginning to the end of the observing period. ALBUS utilizes two ionospheric models, in either 2- or 3-dimensions, and allows for either simply taking a standard model or using the RINEX data themselves to inform the model. The two ionospheric models employed are either the International Reference Ionosphere (IRI) [B2022] and the Parameterized Ionosphere Model (PIM) [D1995]. The program allows for ten different types of models to be created, labelled G00 through G09. ALBUS also utilizes the F10.7 GHz solar flux density values and satellite-measured magnetic field adjustments as needed for these models.

Finally, ALBUS takes the models of the ionosphere and applies them to specific observing directions over time, to create the estimate of IFRM in those directions and at those times. In this final step, as noted previously, ALBUS uses the standard magnetic field model IGRFv13.

We have made ALBUS available within AIPS (under Linux only) by taking the github repository [W2014] directly, and making the call to the highest level Python function *(process_ionosphere)* available from within AIPS through use of a container (https://apptainer.org). The container is built by using the Dockerfile that is provided in the repository. The AIPS task (also called ALBUS) is currently only available locally on computers within the DSOC, and only by request to E. Greisen. ALBUS can, however, be run as a standalone package. It can be compiled following the installation instructions at this site: https://github.com/twillis449/ALBUS_ionosphere/blob/master/INSTALL.

In the following comparisons, we have utilized two versions of ALBUS: The one labelled 'minimal' employs a restricted set of nearby ground stations, while the one labelled 'extended' utilizes a much larger set. These versions differ only in which sites are being queried for obtaining the ground stations data. For the minimal computations, data from the Scripps Orbit and Permanent Array Center (SOPAC, operated by the University of California San Diego) were used as the source of the ground station data. For the extended computations, an additional source of data, from the National Geodetic Survey, operated by NOAA, was included.

6 Imaging

Imaging the low brightness lunar emission, especially with the ~ 30 minute integration times needed to track changes in the IFRM, is challenging for the VLA at meter wavelengths. The primary difficulties are due to external RFI and to signal coupling between antennas – a form of internal RFI. Both are particularly troublesome at the lower frequencies, where the polarized emission is weakest and the IFRM effects we are trying to measure are greatest, and for spacings less than ~ 300 meters – the spacings containing the most information on the lunar emission. We note that these external and cross-coupling signals do not destroy the desired lunar visibility information – they add unwanted correlations of much higher amplitude and incorrect phases. Actual removal of these unwanted correlations is not possible – we can only flag (blank) visibilities deemed to be too corrupted to be worth retaining. Determining the levels at which flagging should occur is more art than science. We have adopted a procedure which removes observed visibilities with amplitudes a few times higher (or lower) than those expected from the lunar emission.

Following the flagging and calibration steps, images were made with a 1 to 1.5 kilowavelength taper, resulting in resolutions of typically three arcminutes. Stokes I, Q, and U images were generated on a timescale of typically 30 minutes to enable tracking of the IFRM changes for the 'D2' and 'DC' observations. Standard 'CLEAN' deconvolution was applied to remove the effects of the PSF.

The lunar EVPA offsets were determined from the Stokes Q and U images by the AIPS program MARSP. The program determines the deviation of the observed EVPA from radial for each image cell. These values are then averaged to produce the mean deviation, and calculates basic statistics to allow error estimation[5].

Examples of the lunar images, using the 'C3' data, at 424 MHz, are shown in Fig 2, with 90 arcseconds resolution. The IFRM from the 'minimal' ALBUS solution has been applied to the data. The Stokes 'Q' and 'U' images are shown in the left two panels. The EVPA of the polarized emission is given by $0.5 \arctan U/Q$. The polarized brightness is shown in the third panel. As expected, it is zero at the lunar center and maximizes near the limb. The isolated

[5]MARSP gets into trouble when the radial deviations approach 90 degrees (as 91 degrees is represented by -89 degrees). The easy fix is to invert both the 'Q' and 'U' images – equivalent to subtracting 90 degrees to all EVPAs. Ninety degrees is then added to the resulting solution.

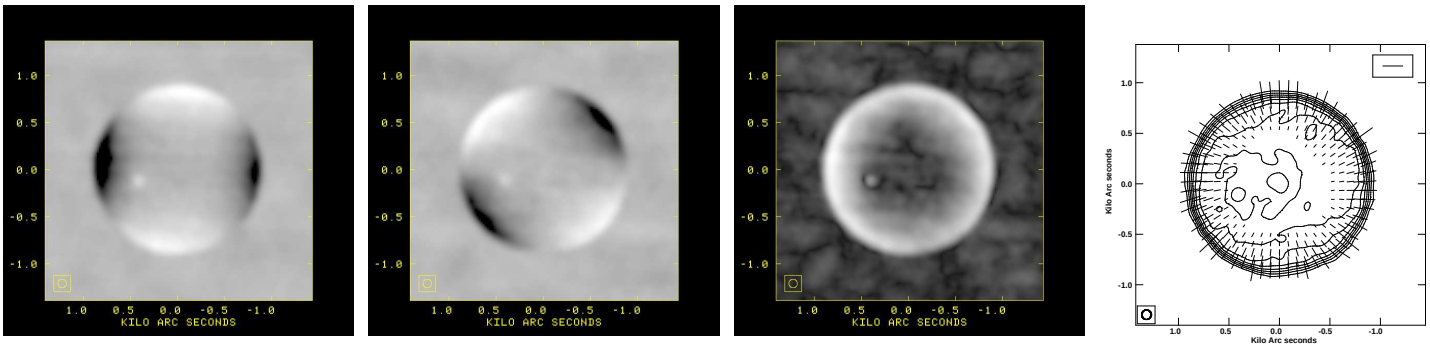

Figure 2: Showing the polarized emission images from the C3 observation, with 90 arcseconds resolution. From left to right: Stokes 'Q', Stokes 'U', polarized intensity, and a contour image of Stokes 'I', with overlaid vectors showing the orientation and fractional polarization of the linearly polarized brightness.

spot of polarized brightness seen on the left side of polarization images, near the center, is solar emission reflected from the lunar surface. The peak polarized brightness is 40 mJy/beam, and the rms noise is 1 mJy/beam. The rightmost panel is a contour plot of the Stokes 'I' brightness, with superposed vectors showing the EVPA orientation and fractional polarization. The maximum fractional polarization is 20%, and the EVPA is nearly perfectly radial, indicating the IFRM estimations are correct.

7 Results

7.1 The IFRM Offset

EVLA Memo#230 demonstrated that the jplg VTEC maps are effective at removing the diurnal changes in IFRM due to solar heating of the ionosphere. However, it was also shown that the applied corrections were too high by a nearly constant amount. The implication was that the estimated IFRM is offset by a nearly constant value, typically 0.5 to 1.0 rad/m^2.

We reproduce from that memo the evidence for this conclusion, taken from our D2 observation. Figure 3 shows the uncorrected, and IFRM corrected, EVPA values for the highly polarized hotspot in DA240 (left panel) and the Moon (right panel). The data and fits in the upper portion of each plot show the time-sequenced uncorrected EVPAs as a function of λ^2 for each observation. The changing slopes reflect the changing values in IFRM. The lower, overlapped, traces in each panel show the result of applying the TECOR IFRM model utilizing the jplg VTEC maps. The remarkable 'condensation' of the corrected EVPA data to a common slope shows that the jplg IFRM estimate has removed the changing portion of the IFRM very well. But the resulting common slope for each source is incorrect. For DA240, the known correct value (from observations made with the WSRT) is 3.04 rad/m^2, while for the Moon, the correct value is 0.0 rad/m^2. For both sources, the application of the jplg IFRM estimates has overcorrected the EVPAs by $\sim 0.6 - 0.7$ rad/m^2.

A negative RM offset in the corrected data, when using the jplg global TEC maps for the Moon, is seen in all six of our lunar observations. The offsets are not the same for each observation – they vary from -0.5 to -1.0 rad/m^2. The same overcorrections are also seen in all observations of DA240 and 3C345, where we take the WSRT observations of Brentjens as the correct values. Similar, but smaller, offsets are seen in the other six global VTEC maps that we tested.

7.2 Comparing Regional ALBUS to Global TECOR models

We noted above that the thin shell models utilizing global VTEC-based maps effectively remove changes in the IFRM due to diurnal solar heating, but also add a nearly constant IFRM offset. Figure 3 demonstrates that the accurate removal of these diurnal changes is not a sufficient condition to conclude that these models are correct, as we clearly see there is an apparent offset in the calculated value of the IFRM. This is why observations of a source of a-priori known EVPA as a function of frequency are needed to judge the correctness of the IFRM estimates.

The most effective comparisons are made using P-band observations of the Moon taken during day–night, or night–day transitions. Two of our observations – 'D2' and 'DC' – are especially suited to this, as both span a day-

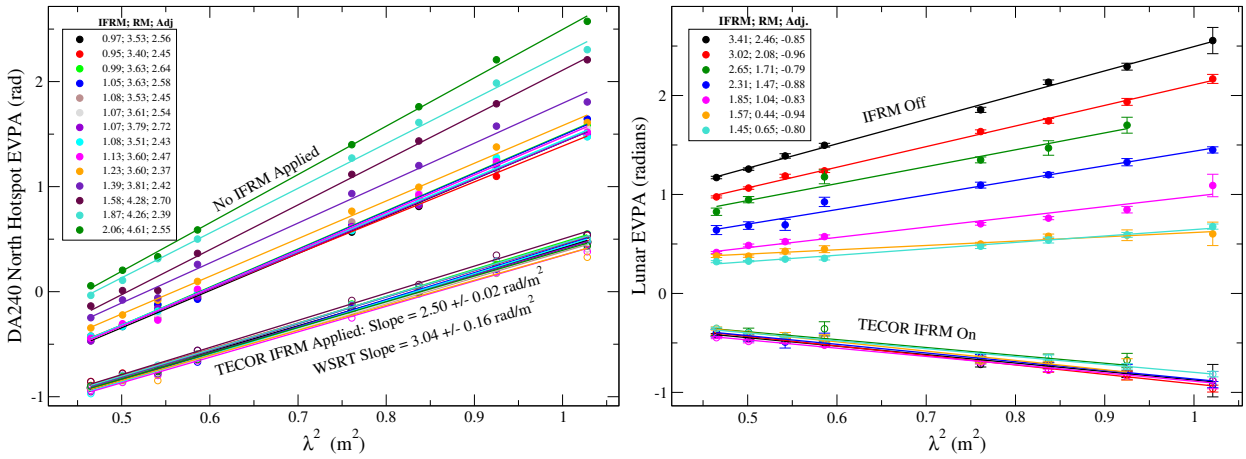

Figure 3: The observed, and IFRM-corrected, EVPAs for DA240 (left) and the Moon (right), using the D2 dataset. For both panels, the data without the IFRM corrections are shown in the upper half of each plot, while the data with the IFRM corrections applied are plotted below. For both sources, the corrections are very effective in removing the effects of the changing ionosphere, as evidenced by the overplotting of the corrected values. However, for both sources, the resulting EVPAs show an apparent, negative residual RM, of ~ -0.7 rad/m^2. See the text for details.

night transition with a significant change in IFRM, and are also taken during apparently calm ionospheric conditions. To make these comparisons, we made 'Q' and 'U' images of the lunar emission for each scan (typically 20 minutes duration) in these two observations. These images allow us to track the time evolution of the IFRM.

Results from the D2 observation are shown in Fig 4. The left panel shows the EVPA deviations from radial for

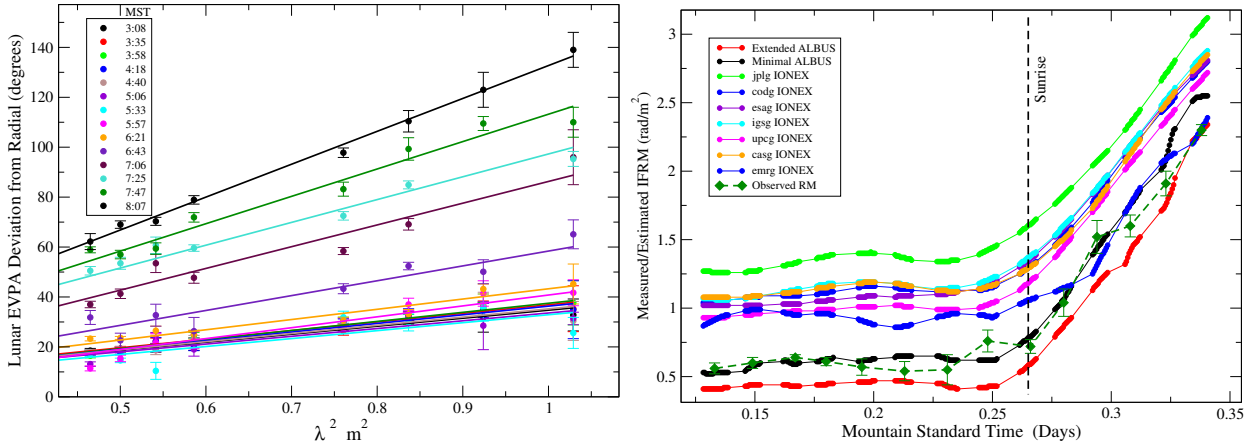

Figure 4: **Left:** The fits to the observed lunar EVPA radial offsets. The slopes are the observed IFRMs. The overlapped data and fits at the bottom of the plot are from the night-time data, the separated, steeper plots are from observations after dawn. The legend gives the local time of the observation. **Right:** Showing the model and observed IFRMs. The 'segmented' traces are the various model values, identified in the legend, while the green diamonds with 1-σ error bars, connected by dashes, are the observed IFRM values from the fits shown in the left panel.

each lunar observation. (These data are essentially the same as those shown in the right panel of Figure 2). The slopes of each time-sequenced observation directly give the IFRM, since we know that the Moon has an intrinsic zero EVPA rotation measure. The observations taken before 06:20 MST are before dawn, and show no significant change in IFRM. After dawn, the observed EVPAs increase as the ionospheric IFRM increases. The values of the slopes in the left-hand panel are plotted in the right-hand panel as the green diamonds, connected by a dashed line, with the estimated $1-\sigma$ error bars. The segmented, solid points in this panel show the IFRM predictions from the seven global, and two ALBUS, models that we tested.

An important point of emphasis is that all the model IFRMs show nearly the same *change* in IFRM as the

solar UV-emission heats the ionosphere. Use of any of these models will then do an excellent job in enabling good polarimetric images. However, it is also clear from this plot that only the two ALBUS models (in red and black) give values close to those actually observed – as shown by their overlap with the dashed green line representing the observed values. All global models have overestimated the IFRM by values varying from 0.4 to 0.7 rad/m^2, values which are remarkably constant over the time of observation. Of the global models, the jplg map (in green) has the greatest overcorrection.

The same exercise has been performed on the 'DC' database, with the results shown in Fig 5. The 'DC' data

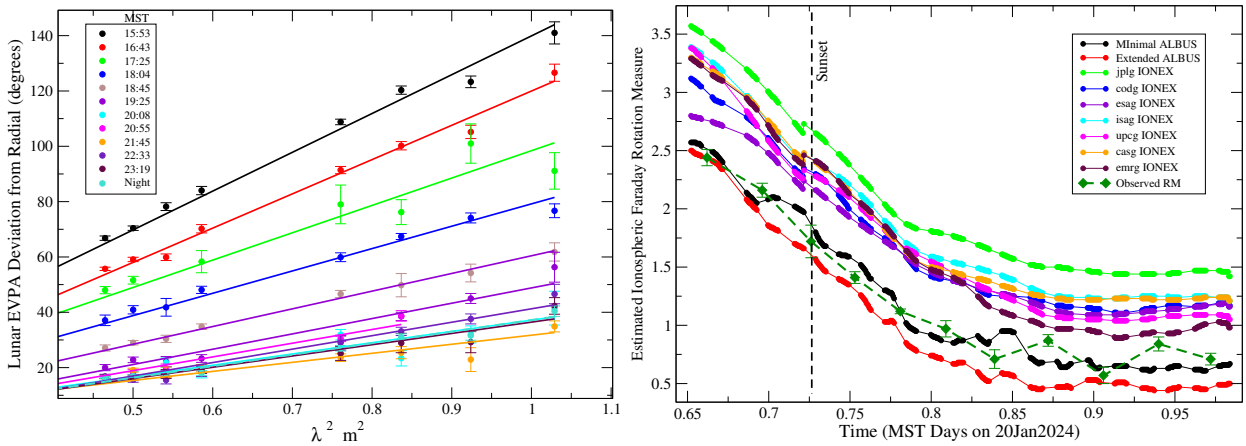

Figure 5: **Left:** The fits to the observed lunar EVPA for the 'DC' data, taken Jan 20, 2024. The slopes are the observed IFRMs. **Right:** The model IFRMs, and the observed IFRMs from the fits, shown in green diamonds.

support the same conclusions as derived from the 'D2' data – all models remove the diurnal change in IFRM with good accuracy, but all global models overestimate the IFRM by a constant amount, while the ALBUS model does the best in matching the observed IFRM values.

The other four observations (D1, C1, C2, and C3) support these conclusions. However, because the changes in IFRM for these observations were smaller than for the D2 and DC observations, we have not attempted to determine the IFRM for each scan. We can however easily determine the IFRM during the night-time hours when the ionosphere is relatively unchanging, and compare these values to the IFRM predictions from the various models. The results of this exercise are shown in Fig 6. It will be seen in this figure that while the conclusions noted above are supported by these observations, there are variations between the days. In particular, the 'C1' observation (upper right panel) shows that the observed IFRM night-time value is more than 0.1 rad/m^2 lower than the ALBUS model determinations, which it will be noted are only slightly less than most of the global models. We are not aware of anything unusual about this particular observation. It will also be noted that the jplg global model predictions (green traces) are the highest for all six observations.

7.3 Comparing RMextract and TECOR

ASTRON has developed its own software to provide IFRM estimates using the same global model VTEC maps that TECOR utilizes. To compare the RMextract predictions to those provided by TECOR, we show in Fig 7 the lunar IFRM predictions for the D2 observation for both TECOR and RMextract, using the jplg and uqrg VTEC maps. The uqrg maps are provided by the Polytechnic University of Catalonia, and differ from the upcg maps by being estimated on a 15-minute cadence, rather than the two hours for upcg.

TECOR, using the jplg VTEC map, provides the estimates shown in green. The black trace shows the RMextract solutions using the same VTEC map. It will be noted there is agreement between them only once every two hours (at 10, 12, and 14 IAT), which are the times at which the map values are defined. TECOR interpolates between map times by assuming the ionosphere remains fixed w.r.t. the Sun, so the task applies time corrections to the apparent longitude while interpolating between map table values[S1998]. This procedure appears to work well, as judged by the resulting smooth curves. In contrast, it appears that RMextract does not apply this rotation correction.

ASTRON recommends the use of the uqrg VTEC maps for IFRM estimates. The TECOR and RMextract estimates using this map are shown in the blue (TECOR) and red (RMextract) traces. The issue of interpolation is largely avoided here because the uqrg maps are on a 15-minute cadence. Close inspection of the red trace shows

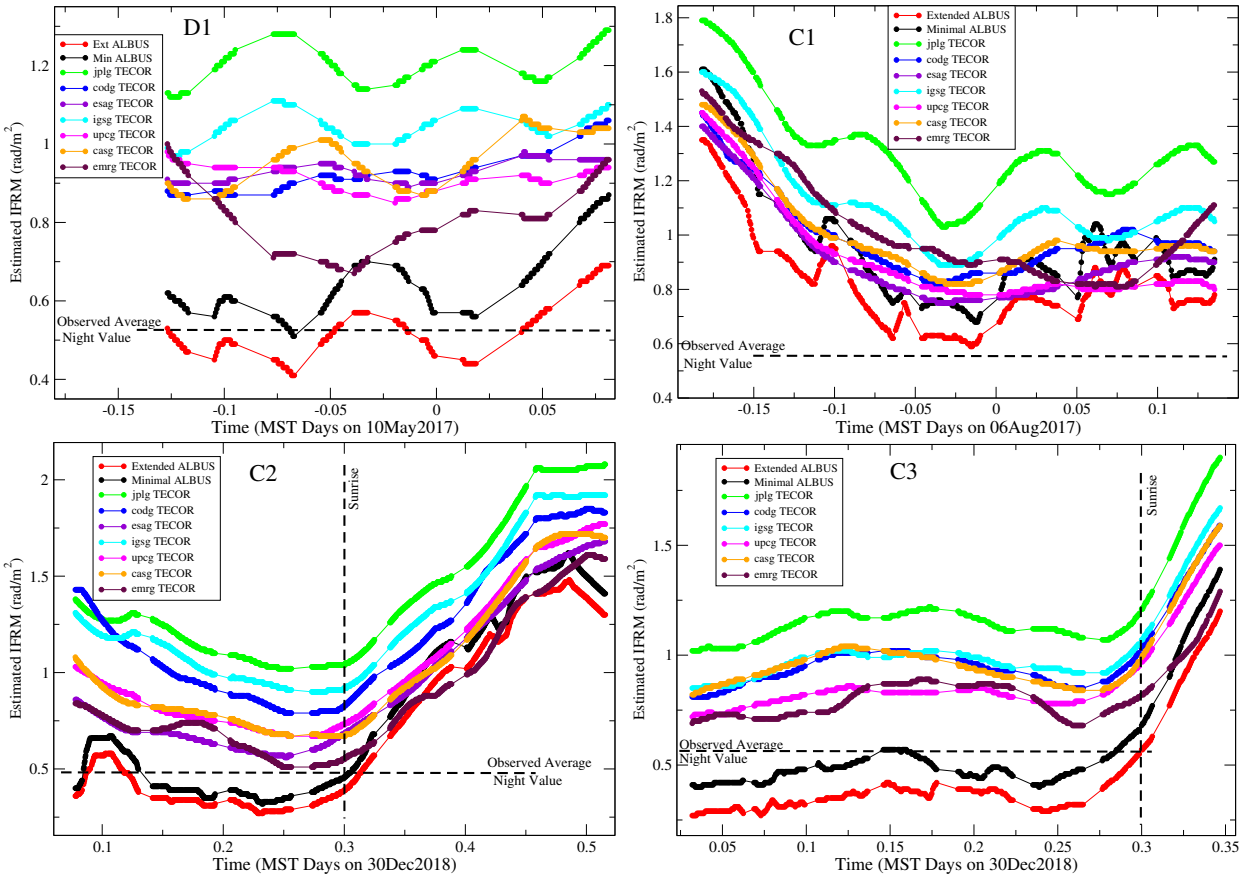

Figure 6: Showing the calculated IFRMs for the various global (TECOR) maps, and the ALBUS regional model estimates. The horizontal dashed line in each panel shows the observationally-determined values of the IFRM during the stable night-time hours. For all six observations, the ALBUS models (in red and black) predict values much closer to those observed than any of the global models.

the inflection points every 15 minutes, corresponding to the times at which the maps are updated. The agreement with the TECOR result is now very good. The ASTRON recommendation is likely based on both this and on the observation that the IFRM offset is less for the uqrg maps than for the jplg maps.

For comparison, the ALBUS model predictions are shown in magenta. These track the actual IFRMs very well, showing that, as for all our observations, the actual IFRMs lie below the global model estimates by a nearly constant value.

7.4 Comparing 'minimal' and 'extended' ALBUS

We tested the ALBUS predictions using two different sets of ground stations, labelled 'minimal' and 'extended'. See the discussion in Section 5.2 for the difference between the two. The intent was to try to determine the optimum number and location of stations which would give the best results. In Table 3 we show the differences between the IFRM solutions and the observed values, utilizing only the data taken at night under fairly calm ionospheric conditions. In this table, the '#Sta' columns give the number of ground stations used in the model, and the columns headed by 'IFRM' give the model and observed IFRM values. In each column, the better IFRM estimate is shown boldfaced. Examination of the values in this table show that the 'minimal' model provides better IFRM estimates than the 'extended' model in four of the six observations. We do not understand why this is.

7.5 Comparing ALBUS models

ALBUS enables ten different ionospheric models, briefly described in Table 4. We have generated the IFRM solutions for nine of these models (omitting G00), for the 'D2' observation. These model predictions are shown in Fig 8. The

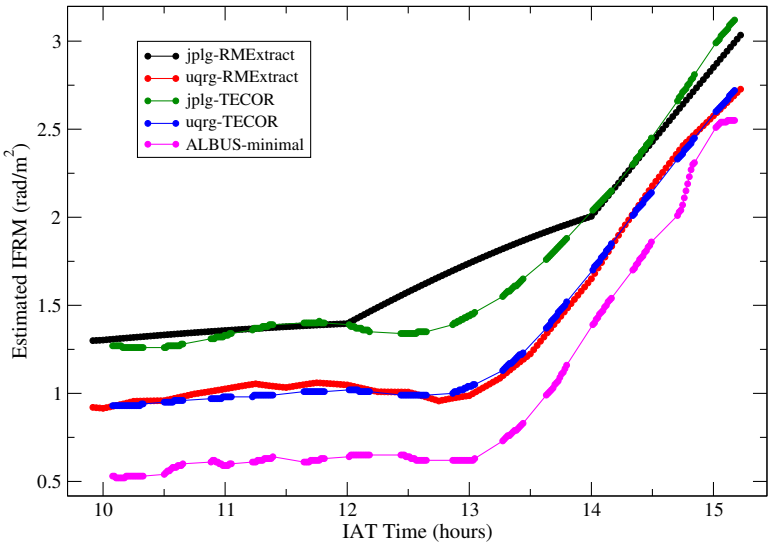

Figure 7: Comparing the IFRM estimates provided by TECOR, RMextract, and ALBUS for the D2 observation. The TECOR solutions using the jplg VTEC map is shown in green, and the uqrg model shown in blue. The RMextract solutions for these two models is shown in black and red. The ALBUS solution – which closely follows the observed IFRMs – is shown in magenta.

Table 3: **Comparison of ALBUS Solutions**

	D1		C1		C2		C3		D2		DC	
Model	#Sta	IFRM	#Sta	IFRM	#Sta	IFRM	#Sta	IFRM	#Sta	IFRM	#Sta	IFRM
jplg	-	1.20	-	1.20	-	1.30	-	1.15	-	1.30	-	1.50
'Minimal'	9	0.70	6	**0.71**	5	0.38	3	**0.52**	3	**0.55**	4	**0.75**
'Extended'	13	**0.50**	12	0.88	11	**0.43**	10	0.38	11	0.37	10	0.57
Observed	-	0.53	-	0.56	-	0.49	-	0.57	-	0.55	-	0.75

three '3D' models (G03, G04, G05) all give identical results. Of the '2-D' models, G02 and G06, and G07 and G08 also give identical solutions.

Comparing these solutions to the observed IFRM values shows that the '3D' model predictions match the data better than any of the '2D' solutions. Consequently, all results presented in this memorandum utilize the '3D' model.

8 Summary and Discussion

Six observations of the Moon with the VLA's P-band receivers have allowed accurate determination of the ionopheric Faraday rotation of the lunar polarized emission as a function of time and wavelength. These observations have permitted accurate comparisons of the actual Faraday rotation to estimates made on the basis of global and regional models. The results of these comparisons allow the following conclusions:

1. All models – global and regional – show similar changes in IFRM between night and day. These changes match well the observed changes in IFRM made from the lunar observations.

2. All global models (as implemented in TECOR and RMextract) overpredict the IFRM by a roughly constant amount, typically from 0.4 to 1.1 rad/m^2. The offset is different on different observation days, but is nearly constant throughout any one day, and varies only slightly between sources on a given day.

3. The thin shell models using the jplg global VTEC maps have the highest overcorrection of all of the thin shell models. Thin shell models using the emrg global VTEC maps usually, but not always, have the lowest overcorrection.

Table 4: **Description of ALBUS Ionosphere Models**

Model	Description
G00	Single station, nearest satellite
G01	Single station, all satellites
G02	Multiple stations, simple 2D
G03	Multiple stations, 3D model (same lat,long for all h)
G04	Multiple stations, 3D model (different lat,long for all h)
G05	Multiple stations, 3D model spherical harmonics with different h layers
G06	Multiple stations, 2D model with time dependence
G07	Multiple stations, 2D model with gradient least squares
G08	Multiple stations, 2D model with time, gradient least squares
G09	Multiple stations, 3D model spherical, gradient least squares

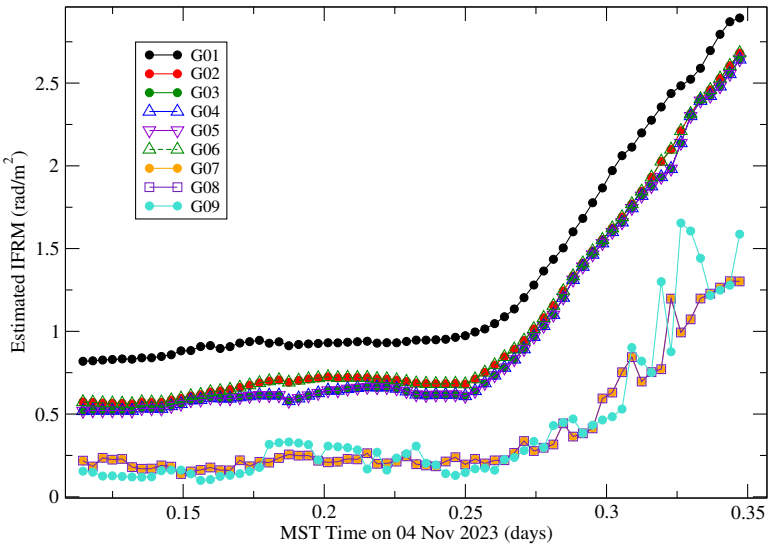

Figure 8: Showing the calculated IFRMs from nine ALBUS models, for the D2 database.

4. The regionally-based ALBUS '3D' models match the observed IFRMs quite well, typically within 0.1 – 0.2 rad/m^2, without any evident constant offset in the IFRM for five of the six observations.

It is important to emphasize that these conclusions are valid only for observations made with the VLA. It is not known if similar conclusions apply for MeerKAT or WSRT data. We do have a single MeerKAT lunar observation, but these data were taken overnight, on a day when the IFRM was extremely low and constant. For this observation, the jplg global VTEC maps estimated an IFRM of $-0.2\,\mathrm{rad/m^2}$, changing by less than $0.05\,\mathrm{rad/m^2}$ over the four-hour duration of the observation.

The origin of the IFRM offsets in the thin shell models using global VTEC maps is unknown. We do know that it is not due to differences in the global magnetic field model, but arises directly from the provided VTEC maps. The ALBUS VTEC estimates are always lower than those provided by the global models. There are references in the geophysical literature on this same conclusion [L2021, W2021, Z2021]. These papers suggest the overestimation of the VTEC may be due to unmodelled latitudinal gradients. There are also suggestions that the thin shell model, used in all of the implementations utilizing these global VTEC maps, is responsible.

We do not understand how ALBUS actually does its model fits. We presume the differences between ALBUS' 3D models and the global VTEC-based maps arise from ALBUS' use of a realistic three-dimensional electron density distribution, combined with it being a regional, rather than global, model. We are now engaging with the software author, (who has long ago left astronomy), to better understand what is going on 'under the hood.'

Similarly, we do not understand the origin of the differences between predictions made by the 'minimal' and 'extended' ALBUS model calculations. The latter uses many more ground stations, inclusion of which we would naively expect would product better models. A possibility for the failure to do so may be related to the absence of

DCB corrections for these additional ground stations in the codg IONEX files.

Although we are confident in our conclusions given above, our determination of the accuracy of the modelling is limited by the relatively short time periods of the six observations. Much more useful would be a full 24-hour observation of known strongly polarized compact calibrators, taken on a day when the solar-induced increase in IFRM is fairly large. We are hopeful in obtaining such an extended observation early next year.

References

[A2021] Alken, P. et al. 2021, Earth Planets Space, 73, 49.

[B2022] Bilitza, D. et al. 2022, Reviews of Geophysics, 62.

[D1995] Daniell, Jr. et al. 1995, Radio Science, 30, 1499.

[E2001] Erickson, W.C. et al. 2001, A&A, 366, 1071.

[G2003] Greisen, E.W., 2003, ASSL, 285, 109.

[L2021] Li, Z., Wang, N., Liu, A. et al. 2001 Satell Navig, 2, 19

[M2018] Mevius, M., 2018, ascl.soft. ascl:1806.024

[PB2013] Perley, R.A., Butler B.J., 2013, ApJS, 206, 16.

[PG2024] Perley, R., Greisen E.W., 2024, EVLA Memorandum #230.

[S1998] Schaer, S.W., Gurtner, W., & Feltens, J. 1998 in Proc. of the 1998 IGS Analysis Centre Workshop, ESOC, Darmstadt, Germany, 233

[S2013] Sotomayor-Beltran, C. et al. 2013, A&A, 552, A58.

[W2021] Wielgosz, P., Milanowska, B., Krypiak-Gregorczyk, A. et al.,2021 GPS Solutions 25, 103.

[W2014] Willis, A., 2014, https://github.com/twillis449/ALBUS_ionosphere.

[Z2019] Zhao, J., Zhou, C., 2019, Annales Geophysicae, 37, 263-271.

[Z2021] Zhao, J. et al. 2021, Journal of Geodesy, 95:35.